JOURNAL OF VIROLOGY, Oct. 2006, p. 10073–10082 Vol. 80, No. 20
0022-538X/06/$08.00+0 doi:10.1128/JVI.01156-06

Asynchronous Progression through the Lytic Cascade and Variations in Intracellular Viral Loads Revealed by High-Throughput Single-Cell Analysis of Kaposi's Sarcoma-Associated Herpesvirus Infection

Laura A. Adang, Christopher H. Parsons, and Dean H. Kedes*

Myles H. Thaler Center for AIDS and Human Retrovirus Research, Box 800734, Departments of Microbiology and Internal Medicine, University of Virginia Health Systems, Charlottesville, Virginia 22908

Received 4 June 2006/Accepted 31 July 2006

Kaposi's sarcoma-associated herpesvirus (KSHV or human herpesvirus-8) is frequently tumorigenic in immunocompromised patients. The average intracellular viral copy number within infected cells, however, varies markedly by tumor type. Since the KSHV-encoded latency-associated nuclear antigen (LANA) tethers viral episomes to host heterochromatin and displays a punctate pattern by fluorescence microscopy, we investigated whether accurate quantification of individual LANA dots is predictive of intracellular viral genome load. Using a novel technology that integrates single-cell imaging with flow cytometry, we found that both the number and the summed immunofluorescence of individual LANA dots are directly proportional to the amount of intracellular viral DNA. Moreover, combining viral (immediate early lytic replication and transcription activator [RTA] and late lytic K8.1) and cellular (syndecan-1) staining with image-based flow cytometry, we were also able to rapidly and simultaneously distinguish among cells supporting latent, immediate early lytic, early lytic, late lytic, and a potential fourth "delayed late" category of lytic replication. Applying image-based flow cytometry to KSHV culture models, we found that de novo infection results in highly varied levels of intracellular viral load and that lytic induction of latently infected cells likewise leads to a heterogeneous population at various stages of reactivation. These findings additionally underscore the potential advantages of studying KSHV biology with high-throughput analysis of individual cells.

Kaposi's sarcoma-associated herpesvirus (KSHV), also known as human herpesvirus-8, is the causative agent of several diseases primarily associated with immunocompromised patients, including Kaposi's sarcoma (KS), primary effusion lymphoma (PEL), and multicentric Castleman's disease (6, 9, 37, 57). Intracellular viral load varies by disease type; it is high, for example, in primary effusion lymphomas and low in infected endothelial (spindle) cells in Kaposi's sarcoma lesions (1).

KSHV maintains a biphasic life cycle, and differential protein expression permits the identification and analysis of viral activation. Like other members of the herpesvirus family, KSHV assumes a semiquiescent transcriptional state termed latency in the vast majority of infected cells. Maintenance of the circular viral genome (episome) of KSHV during latency requires the expression of latency-associated nuclear antigen (LANA), encoded by the viral open reading frame 73 (ORF73) (2, 3, 20, 38, 54). An unknown regulatory signal causes the virus to express the replication and transcription activator (RTA), encoded by the immediate early (IE) gene ORF50, thereby initiating lytic replication through a cascade of viral protein expression (25, 26, 28, 44, 45, 52). The final or "late" phase of the viral lytic cycle is characterized by the assembly of progeny virions and the expression of structural proteins, including K8.1, a glycoprotein found on the surface of virions (5, 23, 27, 36, 58). The transition from latency to lytic replication in infected cells likely plays an important role in the pathogenesis of KSHV-associated disease and the transmission of the virus (20, 29, 47).

Cell culture-based models of KSHV infection have inherent limitations that complicate the interpretation of traditional molecular and cellular assays. Importantly, KSHV-infected cultures usually exhibit spontaneous lytic replication, where 1 to 5% of cells have entered the lytic gene cascade (39). Assays on pooled samples, such as DNA array, quantitative real-time PCR, and immunoblots, by default, include both latent and lytic subpopulations, thereby obscuring experimental analyses (8, 17, 32, 43). Since gene expression in lytically infected cells is robust and involves a wide range of genes, the coexistence of the two states of infection precludes a precise characterization of the viral transcriptomes (latent and lytic). As a result, it is difficult to definitively assign functions to putatively latent proteins in the context of whole-virus infection, since traditional analyses reflect the average of cells pooled from these nonhomogenous populations. Our earlier work suggests highly variable levels of infection within cell culture systems (48). The importance of viral intracellular load on KSHV gene expression is currently uncharacterized, but resultant gene dosage effects could potentially play a role in the differential viral gene expression patterns and their potential effects on host cells in KS lesions compared to those in PELs (1, 33). An assay capable of quantifying and characterizing both latent and lytic KSHV infections and their effects on cellular protein expression in individual cells would provide clear advantages in developing a more precise understanding of KSHV biology and pathogenesis.

* Corresponding author. Mailing address: Myles H. Thaler Center for AIDS and Human Retrovirus Research, Box 800734, Departments of Microbiology and Internal Medicine, University of Virginia Health Systems, Charlottesville, VA 22908. Phone: (434) 243-2758. Fax: (434) 982-1590. E-mail: kedes@virginia.edu.

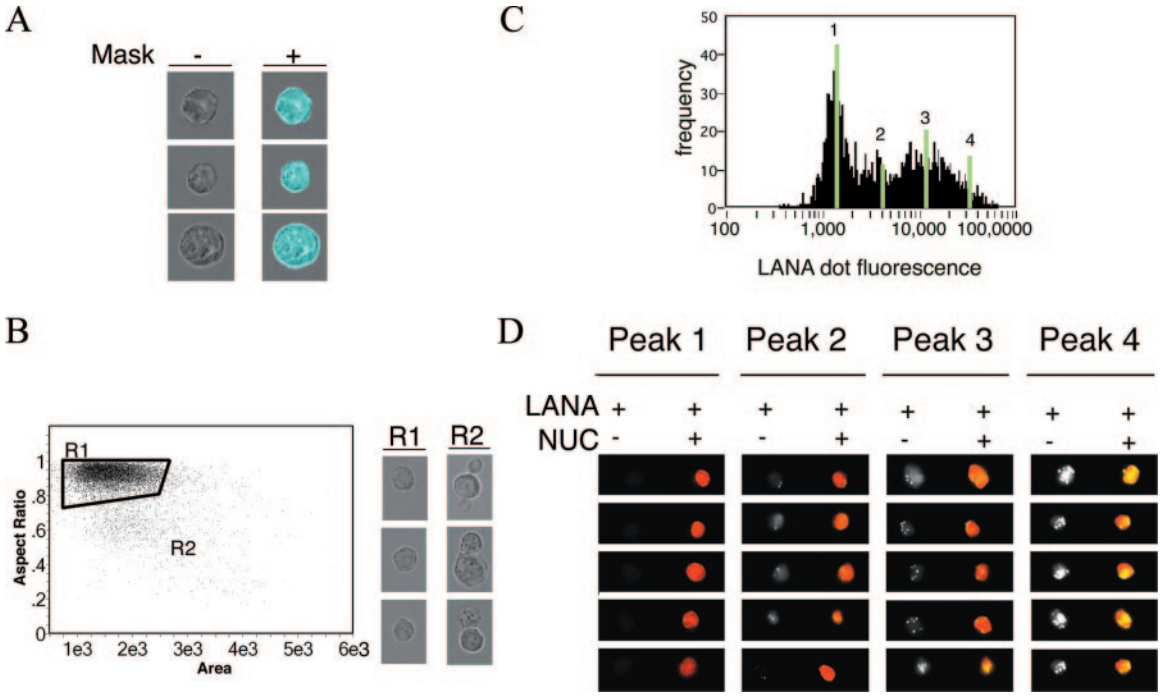

FIG. 1. KSHV-infected HeLa cells are effectively separated by LANA dot fluorescence by use of multispectral imaging flow cytometry. (A) To more accurately measure cell morphological characteristics, the contours of the cells were mapped by creating a mask, as shown in the blue overlay (right column, Mask +) (default bright-field mask eroded by 2 or 3 pixels). Representative cells are shown with and without the mask. (B) Single cells were gated by graphing the mask-corrected parameters of aspect ratio and area. Gate R1 represents nonclumped, single cells, which can be confirmed visually by selecting individual dots in the scatter plot (left column). Aggregated cells, gate R2, were not included in further analyses (right column). (C) A population of KSHV-infected HeLa cells displays heterogeneous LANA dot fluorescence. To determine if the variation in LANA dot fluorescence correlates with nuclear focal maxima of fluorescence, peaks 1 to 4 were selected for further visual analysis. (D) Representative images from cells comprising peaks 1 to 4 indicate that increasing LANA dot fluorescence correlates with increasing LANA dot number. Staining represents DRAQ5 (NUC) and LANA antibody conjugated to Alexa 488 (LANA). The images on the left side of each column, for LANA alone, are shown in black and white. In the superimposed pictures, LANA appears yellow-green over a red nucleus.

To address this issue, we developed a high-throughput assay for the detection of viral and cellular proteins in single cells. We utilized multispectral imaging flow cytometry (MIFC), a new technology that integrates digital imaging with flow cytometry in real time to specifically and quantitatively determine the level of infection within individual cells and to track the phase of the viral life cycle through expression of cellular and viral proteins. We found that de novo infection of naïve populations in culture results in a Poisson-like distribution of viral episomes among the individual cells. In this study, we also investigated the expression of viral and cellular genes in the context of the KSHV life cycle. In stably infected cultures, the analysis of LANA, RTA, syndecan-1, and K8.1 by MIFC allowed high-throughput identification of cells remaining in a latent state while also capturing those undergoing different lytic subphases, including immediate early, early, and late lytic replication, all on a single-cell basis. The latter data revealed that progression through lytic reactivation is also a dynamic and heterogeneous process within the culture.

MATERIALS AND METHODS

Cell culture and viral preparation. BCBL-1 cells were grown in RPMI medium supplemented with L-glutamine, penicillin-streptomycin, sodium bicarbonate, 10% fetal bovine serum, HEPES (pH 7.4), and beta mercaptoethanol as described previously (31). HeLa cells (American Type Culture Collection) were grown in Dulbecco's modified Eagle medium (GIBCO) supplemented with penicillin-streptomycin and 10% fetal bovine serum. KSHV virion production in BCBL-1 cells was induced with 0.6 μM valproic acid (2-propylpentanoic acid); 6 days postinduction, KSHV virions were purified by centrifugation as described previously (31). In brief, virus was sedimented by centrifugation (13,000 rpm for 3 h in a Sorvall Super T21, SL-250T rotor) from media precleared of cellular debris. For the BCBL-1 induction assays, cells were harvested at 24, 48, and 72 h after addition of valproate (0.6 μM), *O*-tetradecanoylphorbol 13-acetate (TPA) (20 ng/ml), and/or sodium butyrate (300 μM). To infect HeLa cells, concentrated virus (multiplicity of infection of 0.1 to 10) and 8 μM Polybrene (Sigma-Aldrich) were added to the HeLa media. After 3 h, the cells were washed twice with 1× phosphate-buffered saline (PBS) and then replaced with fresh media. Infected cells were passaged as normal until harvest.

Immunostaining of cells for flow cytometry. Following trypsinization, 2×10^6 to 5×10^6 HeLa cells per condition were washed twice in 1 ml staining buffer (SB; 3% fetal bovine serum, 0.09% sodium azide in PBS). Cells were fixed with fixation buffer (FB; eBiosciences) or 2% paraformaldehyde (Fisher) for 20 min at room temperature (RT), resuspended in 1 ml permeabilization buffer (PB; eBiosciences), and then incubated for 10 min to block nonspecific antibody binding. Rat anti-LANA monoclonal antibody (1:1,000) in PB was added to the cells for 1 h at 4°C. Cells were washed twice with PB, fixed with FB, and resuspended in 100 μl PBS. Prior to sample collection, after fixation, 50 μM DRAQ5 (BioStatus Ltd, United Kingdom) was added to each experimental sample. The results shown in Fig. 1 are representative of multiple independent experiments.

For analysis of the latent-to-lytic switch, 5×10^6 BCBL-1 cells were washed twice with SB, fixed with FB for 20 min at RT, and resuspended in cold methanol while vortexing at a low speed. Cells were then washed twice in SB, with a 10-min incubation step per wash to block nonspecific staining. Anti-LANA rat monoclonal antibody conjugated to Alexa 488 was diluted as described above, and K8.1 A/B mouse monoclonal antibody (ABI) was conjugated to Alexa 610-phycoerythrin by use of a Zenon kit (Molecular Probes) and used at 1:400.

Syndecan-1 antibody (CD138) (BD Pharmingen) was purchased preconjugated to phycoerythrin and used at 1:20. Rabbit polyclonal RTA antibody was a gift from D. Lukac and was used at 1:600; secondary goat anti-rabbit antibody conjugated to fluorescein isothiocyanate (Jackson Laboratories) was used at 1:300. All antibodies were diluted in SB and incubated with the cells for 1 h at 4°C, and then the cells were washed twice in SB and fixed in FB for 20 min at RT in the dark. Cells were resuspended in 100 μl PBS and stained with DRAQ5 as described above. The results shown in each figure are for two independent replicates; however, the representative images (see Fig. 3A) are from one experiment.

Annexin V staining was conducted as described by the manufacturer (Becton Dickinson), and cells were collected by traditional flow cytometry using a BD FACSCalibur instrument. The results are from three (24-h, 48-h, and 72-h) and four (0-h) independent experiments and are given as means ± standard errors of the mean (SEM) as follows: for 0 h, 9.7% ± 3.3%; for 24 h, 11.2% ± 1.4%; for 48 h, 8.4% ± 2.0%; and for 72 h, 13.0% ± 4.9%. Annexin V staining was performed separately from the MIFC experiments. Syndecan-1 expression levels following TPA and sodium butyrate treatments were measured following antibody staining as described above and were determined in duplicate; the error bars represent ranges. These data were collected by use of a BD FACSCalibur instrument. The value for syndecan-1 expression without induction was 89% ± 1%. For the treatments with sodium butyrate alone, TPA alone, and TPA and sodium butyrate combined, the values were, respectively: for 24 h, 81% ± 4%, 85% ± 2%, and 78% ± 3%; for 48 h, 87% ± 5%, 80% ± 3%, and 73% ± 5%; and for 72 h, 88% ± 6%, 67% ± 2%, and 56%± 6%.

Cell sorting and multispectral imaging flow cytometry. Cells were sorted on a four-stream Becton Dickinson FACSVantage SE turbo sorter with Diva option. MIFC was performed on an ImageStream100 (Amnis Corporation, Seattle, WA) using the manufacturer's collection program, IDEAS (14). Fluorometric compensation was digitally calculated by analysis software (INSPIRE; Amnis Corporation) based on single-stain controls. The data were analyzed according to the manufacturer's instructions by use of INSPIRE software. Briefly, we selected individual, nondoublet cells by comparing the bright-field aspect ratio to the bright-field area. Single cells were rounder (aspect ratio, ~1) and smaller than clumps of cells. Identification of K8.1- and CD138-positive cells was based on selection of distinct cell populations above background fluorescence and confirmed visually by the appearance of cytoplasmic and circumferential fluorescence signals, respectively. The mean fluorescences of LANA dots among infected cells were quantified by the small-spot total intensity analysis, assisted by visual and morphological analysis. Small-spot total intensity (LANA dot fluorescence) is calculated by summing for each cell the fluorescence intensity of focal maxima no greater than 7 pixels (in any contiguous arrangement) after subtracting from each measurement the surrounding background fluorescence (within a 3-pixel radius of each maximum). A spot size of seven contiguous pixels accommodates a single LANA dot regardless of its shape, and the small-spot total intensity algorithm allows the inclusion of LANA dot fluorescence regardless of the proximity of the maxima. The number of dots per cell was manually calculated from a mean of 400 cells per condition to help further validate the automated approach. Total cell area was calculated using the area of each bright-field image eroded by 3 pixels to more accurately reflect cell size. The data presented in Fig. 2 are derived from two independent experiments.

The geometric mean fluorescence intensity of LANA staining and the visually quantified LANA dots per cell shown in Fig. 2C and E are representative of the mean ± standard error of the mean from one experiment. The mean percentage of LANA-positive cells, as determined by LANA dot intensity, and the relative amount of KSHV DNA in each sorted sample are the average values ± ranges ($n = 2$) (Fig. 2D and F).

DNA extraction and quantitative real-time PCR. Following cell sorting based on LANA mean fluorescence intensity, DNA was extracted and ethanol precipitated using standard methods from approximately 2×10^6 to 4×10^6 cells collected from each gate. After resuspension in distilled water, total DNA concentrations were determined using a spectrophotometer (SmartSpec 3000; Bio-Rad, Hercules, CA) by measuring the optical density at 260 nm for each sample to guide the initial normalization of samples added to each PCR.

To measure KSHV DNA within each sample, quantitative real-time PCR experiments amplifying a 67-bp fragment within the latent KSHV gene ORF73 were performed using 200 ng of input DNA in 25-μl reaction mixtures incorporating 0.2 μM of forward (TACTTTACCGGTGGCTCCCA) and reverse (GGGTAAG AGTGCCGGTGGA) primers and 0.1 μM of a sequence-specific TaqMan (ABI) dye-labeled probe (6-carboxyfluorescein–CACCCGCTCCCGCAACACCTTTA C–6-carboxytetramethylrhodamine) (Applied Biosystems, Foster City, CA) with 12.5 μl TaqMan universal PCR master mix (ABI) as previously described (34). To control more precisely for total DNA loaded in each reaction mixture, a portion of the human glyceraldehyde-3-phosphate dehydrogenase gene (huGAPDH) was amplified for each sample in 25-μl reaction mixtures incorporating 50 ng of input DNA with 0.2 μM of forward (CCACCCATGGCAAATTCCA TGGCA) and reverse (TCTAGACGGCAGGTCAGGTCCACC) primers (Operon, Huntsville, AL) with 12.5 μl SYBR green PCR master mix (ABI). Amplification experiments were carried out on an ABI PRIZM 7700 sequence detector, and the resulting amplification plots were analyzed using SDS 1.9 software (ABI). Cycle threshold (C_T) values were tabulated in duplicate for each sample for both KSHV ORF73 and human GAPDH, and water controls were performed to ensure minimal background contamination. By use of mean C_T values, the increase (n-fold) in KSHV DNA amplification for each aliquot relative to the background amplification signal and normalized to huGAPDH was determined using the formula 2^x, where $x = (C_T$ for huGAPDH sample $- C_T$ for ORF73 sample) $- (C_T$ for huGAPDH background $- C_T$ for ORF73 background).

Statistical analysis. Fluorescence data, such as mean fluorescence of LANA dots, are presented in Fig. 3 as the relative geometric mean, with the value for the lowest signal (R1) gate arbitrarily set at 1. Linear correlations were calculated as R^2 values using the Excel spreadsheet program (Microsoft). When the mean values of two independent experiments are presented, the error bars represent the range; otherwise they represent the standard error of the mean.

RESULTS

High-throughput detection and quantitation of LANA dots in individual cells. To measure the levels of infection in individual cells, we employed a fluorometric assay using MIFC, a novel technology that integrates cell microscopy with flow cytometry, creating digital images of each cell as it passes through the detector (see Materials and Methods). Using this approach, we examined the expression of LANA, a latency-expressed viral protein that tethers the viral episome to the host chromatin within the nucleus (2, 3, 13). The assay exploits the distinct punctate nuclear pattern of LANA in KSHV-infected cells and the unique ability of MIFC to combine visible and immunofluorescence microscopy with the statistical power of high-throughput traditional fluorescence flow cytometry. We collected data on infected HeLa cells by MIFC and analyzed the results using the accompanying software package (see Materials and Methods).

Utilizing MIFC's ability to combine flow cytometry with high-throughput imaging, we first employed the system's software to generate a digital cell mask algorithm to more accurately represent cell morphological features (Fig. 1A). This mask contours to the size and shape of each individual cell automatically throughout the population. This application determines, for each identified cell, the characteristics of aspect ratio (roundness) and area. Digitally restricting aspect ratio and area eliminates aggregated cells from further analysis (Fig. 1B). The total intensity of focal maxima of 7 pixels or less (small-spot total intensity) in each cell generated a value that we refer to as LANA dot fluorescence (Fig. 1C). De novo-infected HeLa cells typically displayed heterogeneous numbers of LANA dots per cell—a multiplicity of infection of 1 yielded a range of 0 to 20 or more dots per cell (data not shown). This allowed us to test a range of LANA dots per cell within a single population. Moreover, by compiling the digital images of all the analyzed cells, we confirmed the nuclear localization and numbers of visible LANA dots as a function of LANA dot fluorescence, thereby ensuring the specificity of the assay (Fig. 1D). Visual analysis of cells digitally separated by LANA dot fluorescence (Fig. 1C, peaks 1 to 4) confirmed that the high-throughput determination of spot fluorescence is a reliable

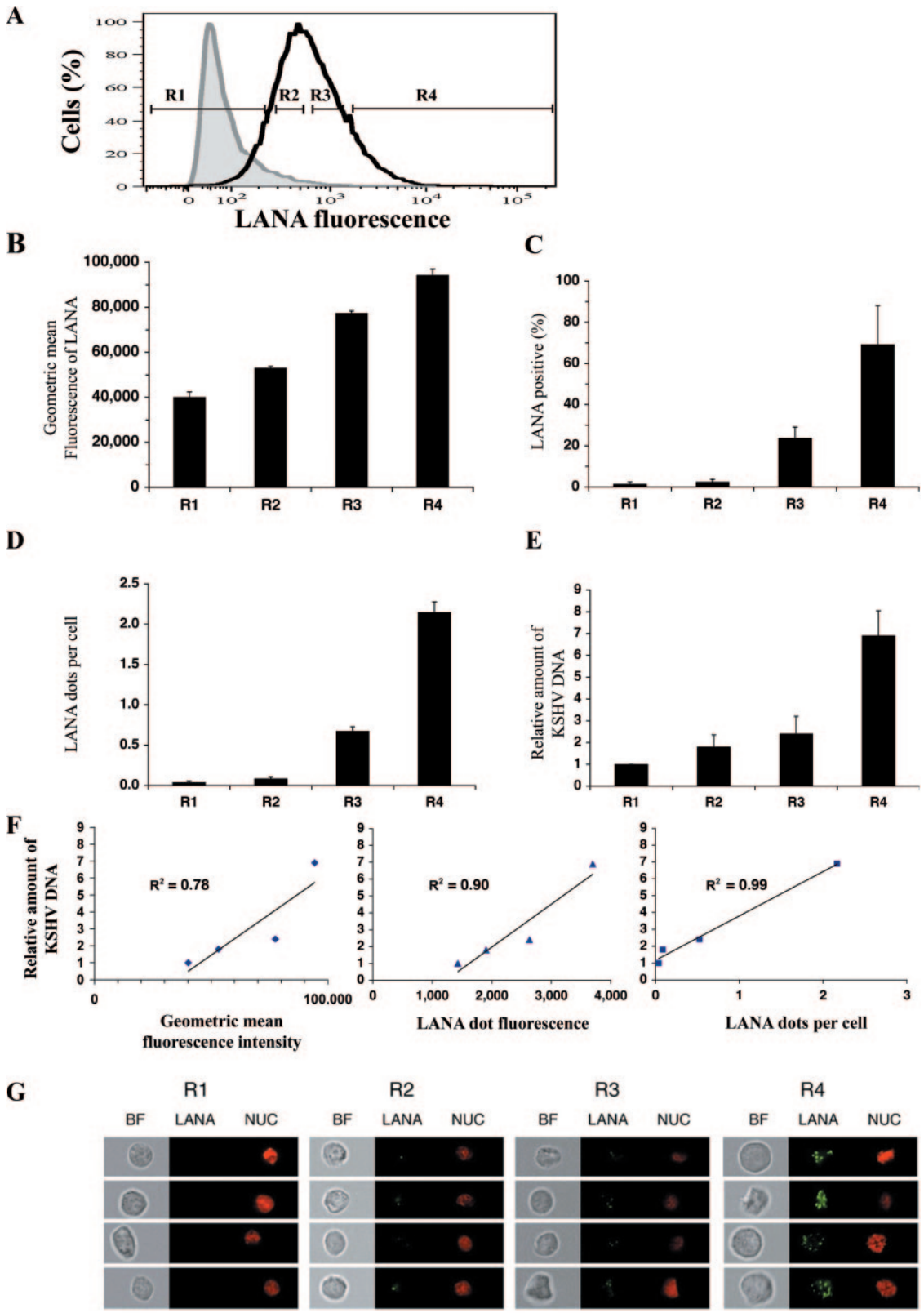

FIG. 2. Number of LANA dots per cell directly correlates with intracellular KSHV DNA. (A) To simultaneously assess the correlation between LANA dots and KSHV episome copy number within a population and test the ability of MIFC to detect low and high frequencies of LANA dots within cells, KSHV-infected HeLa cells were physically sorted into four groups using nonoverlapping gates (R1 to R4) based on LANA fluorescence intensity. Unstained control cells are shown in the shaded overlay histogram. (B) The traditional flow cytometry measurement of the geometric mean fluorescence ± SEM of LANA dots was measured by MIFC in sorted samples. (C) The mean percentage ($n = 2$) ± range of LANA-positive cells was determined

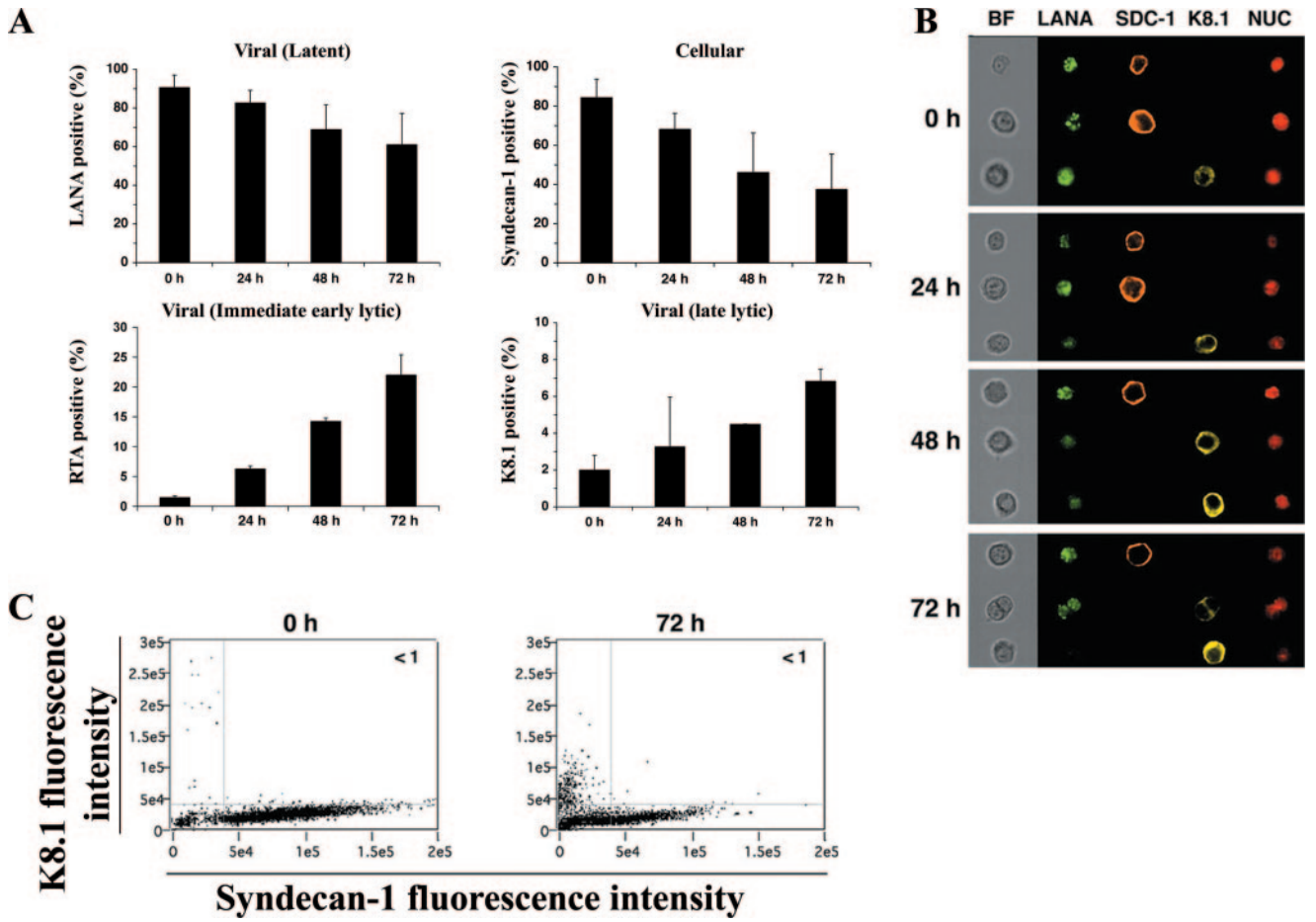

FIG. 3. Characterization of the KSHV latent-to-lytic switch in stably infected BCBL-1 cells. (A) BCBL-1 cells were treated with valproate to induce productive lytic replication. The percentages ± ranges ($n = 2$) of cells positive for syndecan-1, LANA, RTA, and K8.1 following lytic induction were calculated by MIFC. For RTA, values represent means of samples ± standard deviations ($n = 2$ for 24 and 48 h; $n = 4$ for 0 and 72 h). (B) Representative images of BCBL-1 cells 0, 24, 48, and 72 h after valproic acid induction of the viral lytic cycle. Images represent bright-field-masked cells (BF), LANA, syndecan-1 (SDC-1), K8.1, and DRAQ5 (NUC). (C) K8.1 expression is exclusive of syndecan-1 expression at both 0 and 72 h after lytic induction, and less than 1 percent of cells are copositive.

method by which to determine the total numbers of discrete LANA dots (Fig. 1C and D). Importantly, this method can distinguish and digitally analyze subpopulations of cells differing by as few as one or two LANA dots per cell and can do so with a dynamic range of at least 20-fold (Fig. 1 and 2). Our earlier efforts to assess LANA by traditional flow cytometry reliably distinguished only between cells with approximately <2 and those with approximately >40 dots per cell (48).

Multispectral imaging flow cytometry measurement of LANA dots correlates with KSHV DNA. To assess whether LANA dots within individual cells are proportional to the amount of viral DNA and thus verify the use of LANA as a surrogate marker for viral infection, we physically sorted KSHV-infected HeLa cells into four nonoverlapping subpopulations based on LANA mean fluorescence intensity (see Materials and Methods) (Fig. 2A). We then analyzed each subpopulation (R1 to R4) both fluorometrically and visually using MIFC (Fig. 2B to D and G). The geometric mean of LANA fluorescence, the absolute percentage of LANA-positive cells, and the manually calculated mean number of LANA dots per cell within each population (Fig. 2B to D) increased progressively between gates R1 and R4. In parallel, we extracted total DNA from each sorted population and, using quantitative PCR, found that the relative amounts of viral DNA (1, 1.8, 2.4, and 6.9 for R1, R2, R3, and R4, respectively) also

by the percentage of cells with a threshold level of LANA dot fluorescence intensity (see Materials and Methods). (D) The average numbers ± SEM of LANA dots per cell within each sorted population were visually counted. (E) Relative amount of KSHV DNA normalized to cellular GAPDH and arbitrarily set to a value of 1 for gate R1. (F) Relationships between relative amount of KSHV DNA per sorted sample and MIFC measurements of LANA: geometric mean fluorescence intensity ($R^2 = 0.78$), LANA dot fluorescence ($R^2 = 0.90$), and LANA dots per cell ($R^2 = 0.99$). Error bars were omitted for clarity; refer to panels B, D, and E. (G) Representative MIFC images from each gate of bright-field (BF), LANA, and nuclear (NUC) staining. For ease of visualization, we selected images for each category at the upper end of the range of LANA dots per cell.

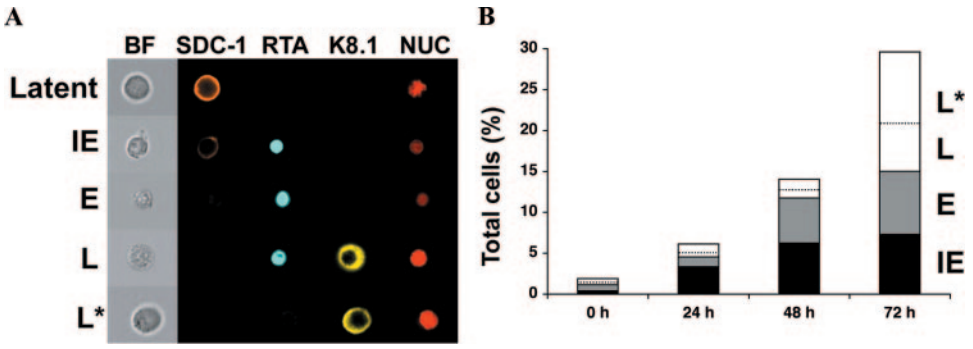

FIG. 4. Visualization of BCBL-1 cells reveals four distinct lytic subpopulations. BCBL-1 cells were lytically reactivated with valproate, and protein expression within individual cells was measured by MIFC. (A) Images representing the distinct phases of syndecan-1 (SDC-1), RTA, and K8.1 expression are shown in addition to images of bright-field-masked cells (BF) and nuclei as stained by DRAQ5 (NUC). Proposed corresponding viral phases are indicated to the left as latent, immediate early (IE), early (E), late (L), and delayed late (L*). Note that there are two distinct populations clustered into the late category. Cells chosen are all from the 48-hour time point. (B) Percentage of BCBL-1 cells in each of the viral lytic subcategories at 0, 24, 48, and 72 h. Black bars represent IE, gray early, and white late. The IE population has its greatest period of expansion between 0 and 24 h, the early population between 24 and 48 h, and the late population between 48 and 72 h.

increased with higher levels of LANA mean fluorescence (Fig. 2E and F).

To characterize more directly the correlation between KSHV DNA and LANA, we next compared the relative amounts of KSHV DNA to three MIFC parameters of LANA expression: (i) geometric mean fluorescence intensity, (ii) LANA dot fluorescence, and (iii) the average number of LANA dots for each of the four subpopulations (Fig. 2A, R1 to R4). Geometric mean fluorescence, a typical output reading of traditional flow cytometry, had the worst correlation with KSHV DNA levels (R^2 of 0.78) (Fig. 2F). In contrast, the high-throughput measurement of LANA dot fluorescence and the manually calculated average number of LANA dots per cell resulted in linear correlations with viral DNA that had markedly higher predictive values (R^2 values of 0.90 and 0.99, respectively) (Fig. 2F).

Tracking the KSHV lytic viral cascade. Following initial infection, KSHV, like all herpesviruses, assumes a prolonged period of latency. Lytic reactivation of the virus, however, is a critical phase in viral pathogenesis, as it leads to progeny virion production, horizontal spread, and viral transmission, as well as the expression of potentially pathogenic lytic genes (17). To explore the ability of MIFC to differentiate between the phases of viral reactivation, we chemically induced the latently infected primary effusion lymphoma cell line BCBL-1 with valproic acid and measured expression of the essential latent protein, LANA; the lytic switch protein, RTA; and the late lytic marker, K8.1, at hours 0, 24, 48, and 72 (Fig. 3) (5, 23, 36, 42, 56). Prestimulation, RTA and K8.1 were each present in approximately 2% of cells, consistent with spontaneous lytic replication (Fig. 3A, bottom panels). By day 3 poststimulation, however, RTA and K8.1 were present in 23% and 7% of the total population, respectively (Fig. 3A, bottom panels). Of note is the fact that the percentage of cells positive for LANA dots decreased over this same 3-day period by ~30% (91% at 0 h, 83% at 24 h, 69% at 48 h, and 61% at 72 h) in rough correspondence to the number of lytic (RTA^+) cells in the population (Fig. 3A, upper left panel). Moreover, this decrease in LANA did not correlate with an increase in cell death, as shown by annexin V staining (see Materials and Methods) (49).

Syndecan-1 is present during immediate early lytic replication but absent during the late lytic phase. We also examined BCBL-1 cells for their levels of expression of syndecan-1 (CD138), a cell surface protein that serves as a biomarker for diagnosing KSHV-associated and other lymphomas (10). Syndecan-1 staining markedly decreased following lytic induction, a finding we confirmed visually (Fig. 3A and B). In individual cells, K8.1 and syndecan-1 expressions were mutually exclusive, with or without chemical induction (Fig. 3C). To rule out apoptosis or cell death as the cause of the drop in syndecan-1 expression, we also stained the cells with annexin V, a marker of early apoptosis or necrosis (49). We found that at each of the time points (from 0 to 72 h postinduction) the portion (approximately 10%) of cells staining with annexin V remained statistically unchanged, arguing against cell death as the cause of syndecan-1 downregulation (see Materials and Methods). Moreover, the loss of syndecan-1 expression was not specific to exposure to valproate, since it also occurred following induction by TPA and TPA combined with low-level sodium butyrate (see Materials and Methods). We found that RTA was present in a portion of cells expressing syndecan-1, though the remainder had lost syndecan-1 expression (Fig. 4A). We reasoned that this population of RTA single positive cells (syndecan-1^-/$K8.1^-$) may represent the early lytic replication phase (Fig. 4) marked in these experiments by syndecan-1 downregulation prior to K8.1 expression.

Through the use of syndecan-1, RTA, and K8.1, we were able to simultaneously measure the phases of lytic replication within a single population (Fig. 4B). Specifically, we combined visual and fluorometric analyses through MIFC and distinguished latent ($LANA^+$/syndecan-1^+/RTA^-/$K8.1^-$) from immediate early lytic (syndecan-1^+/RTA^+/$K8.1^-$), presumed early (syndecan-1^-/RTA^+/$K8.1^-$), and late lytic (syndecan-1^-/$RTA^{+/-}$/$K8.1^+$) viral infection among individual cells in a population undergoing dynamic changes among these different stages. We followed each of the stages over time and, consistent with their classification, found that the immediate early

population increased most markedly between 0 and 24 h postinduction (>8-fold increase), whereas the late lytic group increased most between 48 and 72 h (>6-fold increase) (Fig. 4B). The putative early lytic population increased most during the intermediate time period of 24 to 48 h (>4-fold increase) (Fig. 4B).

Although we have designated all cells expressing K8.1 as late lytic in Fig. 4A, we found that over half of these cells did not coexpress RTA (62% at 0 h, 67% at 24 h, 57% at 48 h, and 60% at 72 h). This loss of RTA signal is suggestive of a potential fourth "delayed late" lytic subcategory occurring after the initiation of K8.1 (late lytic protein) expression. This delayed late lytic subpopulation increased in absolute percentage following lytic induction, though the levels of annexin V staining, as we mention above, were statistically indistinguishable during the time course (see Materials and Methods). These latter findings suggest that the loss of RTA expression in this lytic subset was likely not a result of cell death but may instead have identified these cells as ones approaching the final stages of lytic replication.

DISCUSSION

New techniques to evaluate the effect of KSHV in individual cells and qualitatively assess lytic replication are necessary to develop a more through understanding of the virus's biology and pathogenesis. Our adaptation of MIFC to KSHV infection allows for sensitive detection of intracellular viral load as well as quantitative analysis of diverse cellular processes and the asynchronous viral life cycle in single cells. Until now, characterization of KSHV in the laboratory setting has relied primarily on pooled samples of infected cells, which do not reflect the inherent the heterogeneity of KSHV infection.

The paradigm of high-throughput single-cell analysis, traditional flow cytometry, is unable to distinguish among small variations in the numbers of LANA dots per cell and suffers from low overall sensitivity, requiring high numbers of intracellular LANA dots to discriminate infected from uninfected cells (48). Such high levels of infection, however, may be physiologically relevant only in models of primary effusion lymphomas that have high copy numbers of LANA dots (50 or more) on average per cell (1). In contrast, infected cells seen in cases of multicentric Castleman's disease and KS are associated with six or fewer dots (1). To assess intracellular viral load in individual cells, we employed HeLa cells, since they are readily infected by KSHV (in the presence of Polybrene) and display heterogeneity in the number of LANA dots per cell following infection (Fig. 1). The LANA pattern we detected by MIFC is reminiscent of staining that we and others have observed by immunofluorescence microscopy (2, 12, 20, 21). Our data indicate that the automated determination of the total fluorescence of the LANA dots correlates with the viral load in individual cells, validating our sensitive single-cell detection system (Fig. 1 and 2) (34). This approach discriminated among subpopulations differing by as few as one or two dots per cell (Fig. 1D and Materials and Methods). The difference in KSHV detection levels between these two flow-based techniques is due to the ability of MIFC to quantify signal intensities emanating from small, localized maxima of fluorescence such as LANA dots and the tabulation by traditional flow cytometry of the total fluorescence intensity irrespective of the signal distribution within the cells (e.g., cytoplasmic or nuclear, diffuse or punctuate) (14). Since currently available software limits MIFC to single-plane fluorescence microscopy, it remains a formal possibility that this method may not measure LANA grossly out of the center of the cell.

We also exploited the sensitivity and specificity of MIFC to accurately monitor, at the single-cell level, the viral life cycle within a heterogeneous population. In culture systems, chemical agents such as valproate, sodium butyrate, or TPA, as well as transduction with adenovirus-encoded ORF50, induce lytic replication (30, 42, 55). Using the BCBL-1 PEL line, we induced cells to undergo lytic reactivation with valproate and observed a consistent decrease in the fraction of LANA-positive cells that approximated the portion of cells initiating the lytic cascade (Fig. 3B). This contrasts with previous work that has suggested that there is no lytic protein-associated decrease in LANA protein by immunoblotting (30). This discrepancy may be due to the inherent nature of immunoblot analysis, which detects a single signal averaged over an entire population of cells, rendering the technique less sensitive to small changes. Further, in contrast to immunoblotting, MIFC is able to distinguish between diffuse and punctate patterns of LANA signaling, with only the latter form of the protein likely associated with viral episomes (4, 13, 40). A better understanding of this observation of LANA dot loss will require further studies on its mechanism and its physiological implications. Nevertheless, a simple explanation might be that in the later stages of lytic replication, the degradation of LANA may be greater than its synthesis, thereby lowering its concentration to one below the threshold of MIFC detection. Alternatively, LANA in these cells may no longer associate with the host heterochromatin, potentially contributing to a relocalization within the cell and possibly the loss of its characteristic punctate localization. Of note is the fact that Kudoh and coworkers found that EBNA-1, the functional homolog of LANA in the closely related Epstein-Barr virus (human herpesvirus-4), loses its chromatin-tethering function and redistributes within the nuclei following lytic reactivation (22). The assays were limited to cells the investigators followed by fluorescence microscopy, and thus they may not have detected whether a minor subset of the infected cells had lost the EBNA-1 signal at later stages of the lytic cycle.

In this study, we investigated the expression of two lytic viral proteins: the immediate early protein RTA, which initiates the lytic cascade; and the late lytic gene product K8.1, a glycoprotein found on the surface of virions (5, 23, 25–27, 36, 58). The levels and patterns of RTA and K8.1 expression following induction that we observed were similar to those evident in other studies (23, 45, 58). In uninduced cells, ~2% cells expressed RTA, reflecting baseline levels of spontaneous lytic replication (39). MIFC has clear advantages in identifying lytic populations, since it can identify and evaluate individual cells expressing different combinations of viral proteins while providing high-throughput statistical data and visual information, such as protein localization. Moreover, MIFC analysis of the KSHV life cycle is effective without synchronization of viral gene expression.

We wanted to explore the ability of this technique to simultaneously study cellular and viral proteins, but previous reports

have shown that BCBL-1 cells express only a limited number of surface markers (18, 46). Accordingly, we chose to follow syndecan-1, since the fraction of positive cells is greater than 80%, a phenotype that has made it a routine marker to help identify primary effusion lymphomas in clinical isolates (11). The data in this study are the first to demonstrate that syndecan-1 expression depends on the state of the viral life cycle (Fig. 3 and 4). The loss of syndecan-1 expression occurred following the expression of RTA but prior to the expression of K8.1. We assigned the RTA single positive (RTA^+/syndecan-1^-/$K8.1^-$) subpopulation as those cells supporting early lytic gene expression, because the proportion of cells displaying this profile expanded after the immediate early and prior to the late ($K8.1^+$) lytic subpopulation expansions (Fig. 4). The RTA^+/syndecan-1^-/$K8.1^-$ cell category likely reflects the majority of the early lytic population, but better delineation of the transitions between each lytic phase will require further experimentation with an additional array of lytic protein-specific antibodies. Moreover, the focus of this study was on protein expression profiles within the first 3 days after lytic induction in the primary effusion lymphoma cell line BCBL-1. Our results suggest that the initial stages of lytic induction are not associated with an increase in cell death by annexin V staining. Investigation into protein expression profiles at later time points might reveal relevant information on the mechanism(s) of cell death. It is likely that cell death (apoptosis or necrosis) would occur at later times, following the peak of virion release.

Since the absence of syndecan-1 expression was evident in K8.1-positive cells undergoing low levels of spontaneous lytic reactivation, the loss of the cellular protein likely is not due to a nonspecific effect of valproic acid but rather is a direct or indirect viral effect (Fig. 3A and C). Furthermore, the loss of detectable syndecan-1 (and LANA dots) did not correlate with cell death, since the percentage of annexin V-positive cells was statistically unchanged following lytic induction (Fig. 3 and 4 and Materials and Methods). Several possibilities for the potential mechanism of syndecan-1 downregulation exist. One is that that syndecan-1 protein production is specifically decreased by the lytic expression of SOX, encoded by ORF37, which shortens the half-life of targeted cellular mRNAs (15, 16). Alternatively, syndecan-1 may be actively downregulated at the surface of the cell by a viral ubiquitin E3 ligase, such as MIR1 (ORF K3) or MIR2 (ORF K5) (7, 41). Yet another alternative is that syndecan-1 is shed from the surface of cells. The mechanism underlying syndecan-1 shedding in other settings can involve several proteins, including matrix metalloproteinase-9, a cellular protein potentially upregulated by the lytic virally encoded K1 protein (50). Moreover, all of these viral candidates, SOX, K1, K3, and K5, are expressed after RTA expression and prior to K8.1 expression, conforming to the "early lytic" pattern of syndecan-1 expression that we find during lytic cycle progression. A better understanding of the potential role that loss of syndecan-1 following lytic induction may have in KSHV pathogenesis will require further study, including an initial focus on the underlying mechanism involved.

By monitoring the levels of viral proteins in individual cells, we have potentially identified a fourth lytic subcategory of cells that express the late lytic viral protein K8.1 but have lost RTA expression (Fig. 4A). We hypothesize speculatively that these may be cells supporting the last stages of the productive phase of the lytic cycle and no longer requiring continued initiation of the lytic cycle by RTA. We have named this subcategory the delayed late lytic stage (Fig. 4). The identification of this delayed late population is supported by several other studies which demonstrate the repression of immediate early genes in the later stages of lytic replication (19, 24, 35, 51, 53). Our ability to detect this previously uncharacterized RTA^-/$K8.1^+$ subpopulation may simply reflect the increased sensitivity and specificity inherent in high-throughput analysis of single cells—an approach that avoids attenuation or loss of subtle differences as a result of averaging signals over heterogeneous populations. The functional or mechanistic implications of this lytic phase will also require additional experimentation.

In this paper, we employed a novel high-throughput single-cell methodology to characterize intracellular viral load and progression through the lytic cycle in populations of KSHV-infected cells. The MIFC algorithm that we have devised to detect LANA dot fluorescence specifically and sensitively identifies infected cells even if they are present at low frequencies and further distinguishes these cells based on the level of infection. Moreover, by combining LANA detection with additional viral and cellular protein markers, we used the image-based flow cytometric approach to determine the number (and proportion) of cells undergoing each of the major stages of the lytic gene cascade. Our data argue that even within controlled culture systems, de novo infection with KSHV and its reactivation from latency are complex and heterogeneous processes. As a result, the approaches we have developed in this study should help decipher the interplay between virus and host not only in cell culture but also in in vivo models of KSHV infection and potentially in clinical samples from patients (34).

ACKNOWLEDGMENTS

We especially thank Joanne Lannigan and Michael Solga of the University of Virginia Flow Cytometry Core Facility for technical assistance in the development of these assays. Additionally, we thank David Lukac for the gift of the RTA antibody and Brandon E. Kremer for critical review of this work.

Funding was provided by the National Institutes of Health (5R-01CA88768 to D.H.K. and K08-1CA103858-01A1 to C.H.P.) and the Doris Duke Clinical Scientist Development Award (D.H.K.; 20000355) and through the University of Virginia Cancer Center (P30 CA44579). L.A.A. was supported in part by Medical Scientist Training Grant T32 GM 07267-27 from the NIH and is an ISAC Scholar.

REFERENCES

1. **Asahi-Ozaki, Y., Y. Sato, T. Kanno, T. Sata, and H. Katano.** 2006. Quantitative analysis of Kaposi sarcoma-associated herpesvirus (KSHV) in KSHV-associated diseases. J. Infect. Dis. **193:**773–782.
2. **Ballestas, M. E., P. A. Chatis, and K. M. Kaye.** 1999. Efficient persistence of extrachromosomal KSHV DNA mediated by latency-associated nuclear antigen. Science **284:**641–644.
3. **Barbera, A. J., J. V. Chodaparambil, B. Kelley-Clarke, V. Joukov, J. C. Walter, K. Luger, and K. M. Kaye.** 2006. The nucleosomal surface as a docking station for Kaposi's sarcoma herpesvirus LANA. Science **311:**856–861.
4. **Canham, M., and S. J. Talbot.** 2004. A naturally occurring C-terminal truncated isoform of the latent nuclear antigen of Kaposi's sarcoma-associated herpesvirus does not associate with viral episomal DNA. J. Gen. Virol. **85:**1363–1369.
5. **Chandran, B., C. Bloomer, S. R. Chan, L. J. Zhu, E. Goldstein, and R. Horvat.** 1998. Human herpesvirus-8 ORF K8.1 gene encodes immunogenic glycoproteins generated by spliced transcripts. Virology **249:**140–149.
6. **Chang, Y., E. Cesarman, M. S. Pessin, F. Lee, J. Culpepper, D. M. Knowles, and P. S. Moore.** 1994. Identification of herpesvirus-like DNA sequences in AIDS-associated Kaposi's sarcoma. Science **266:**1865–1869.

7. **Coscoy, L., D. J. Sanchez, and D. Ganem.** 2001. A novel class of herpesvirus-encoded membrane-bound E3 ubiquitin ligases regulates endocytosis of proteins involved in immune recognition. J. Cell Biol. **155:**1265–1273.
8. **Duprez, R., E. Kassa-Kelembho, S. Plancoulaine, J. Briere, M. Fossi, U. Kobangue, P. Minsart, M. Huerre, and A. Gessain.** 2005. Human herpesvirus 8 serological markers and viral load in patients with AIDS-associated Kaposi's sarcoma in Central African Republic. J. Clin. Microbiol. **43:**4840–4843.
9. **Franceschi, S., L. Dal Maso, P. Pezzotti, J. Polesel, C. Braga, P. Piselli, D. Serraino, G. Tagliabue, M. Federico, S. Ferretti, V. De Lisi, F. La Rosa, E. Conti, M. Budroni, G. Vicario, S. Piffer, F. Pannelli, A. Giacomin, F. Bellu, R. Tumino, M. Fusco, G. Rezza, et al.** 2003. Incidence of AIDS-defining cancers after AIDS diagnosis among people with AIDS in Italy, 1986–1998. J. Acquir. Immune Defic. Syndr. **34:**84–90.
10. **Gaidano, G., A. Gloghini, V. Gattei, M. F. Rossi, A. M. Cilia, C. Godeas, M. Degan, T. Perin, V. Canzonieri, D. Aldinucci, D. Capello, G. Saglio, A. Pinto, and A. Carbone.** 1997. KSHV/HHV-8(+) primary effusion lymphoma associates with CD138/syndecan-1 and other plasma cell-specific markers: histogenetic and pathogenetic implications. Blood **90:**4894–4900.
11. **Gaidano, G., A. Gloghini, V. Gattei, M. F. Rossi, A. M. Cilia, C. Godeas, M. Degan, T. Perin, V. Canzonieri, D. Aldinucci, G. Saglio, A. Carbone, and A. Pinto.** 1997. Association of Kaposi's sarcoma-associated herpesvirus-positive primary effusion lymphoma with expression of the CD138/syndecan-1 antigen. Blood **90:**4894–4900.
12. **Gao, S. J., L. Kingsley, D. R. Hoover, T. J. Spira, C. R. Rinaldo, A. Saah, J. Phair, R. Detels, P. Parry, Y. Chang, and P. S. Moore.** 1996. Seroconversion to antibodies against Kaposi's sarcoma-associated herpesvirus-related latent nuclear antigens before the development of Kaposi's sarcoma. N. Engl. J. Med. **335:**233–241.
13. **Garber, A. C., M. A. Shu, J. Hu, and R. Renne.** 2001. DNA binding and modulation of gene expression by the latency-associated nuclear antigen of Kaposi's sarcoma-associated herpesvirus. J. Virol. **75:**7882–7892.
14. **George, T. C., D. A. Basiji, B. E. Hall, D. H. Lynch, W. E. Ortyn, D. J. Perry, M. J. Seo, C. A. Zimmerman, and P. J. Morrissey.** 2004. Distinguishing modes of cell death using the ImageStream ® multispectral imaging flow cytometer. Cytometry Part A **59:**237–245.
15. **Glaunsinger, B., and D. Ganem.** 2004. Highly selective escape from KSHV-mediated host mRNA shutoff and its implications for viral pathogenesis. J. Exp. Med. **200:**391–398.
16. **Glaunsinger, B., and D. Ganem.** 2004. Lytic KSHV infection inhibits host gene expression by accelerating global mRNA turnover. Mol. Cell **13:**713–723.
17. **Hammock, L., A. Reisenauer, W. Wang, C. Cohen, G. Birdsong, and A. L. Folpe.** 2005. Latency-associated nuclear antigen expression and human herpesvirus-8 polymerase chain reaction in the evaluation of Kaposi sarcoma and other vascular tumors in HIV-positive patients. Mod. Pathol. **18:**463–468.
18. **Jenner, R. G., K. Maillard, N. Cattini, R. A. Weiss, C. Boshoff, R. Wooster, and P. Kellam.** 2003. Kaposi's sarcoma-associated herpesvirus-infected primary effusion lymphoma has a plasma cell gene expression profile. Proc. Natl. Acad. Sci. USA **100:**10399–10404.
19. **Jupp, R., S. Hoffmann, R. M. Stenberg, J. A. Nelson, and P. Ghazal.** 1993. Human cytomegalovirus IE86 protein interacts with promoter-bound TATA-binding protein via a specific region distinct from the autorepression domain. J. Virol. **67:**7539–7546.
20. **Kedes, D. H., M. Lagunoff, R. Renne, and D. Ganem.** 1997. Identification of the gene encoding the major latency-associated nuclear antigen of the Kaposi's sarcoma-associated herpesvirus. J. Clin. Investig. **100:**2606–2610.
21. **Kedes, D. H., E. Operskalski, M. Busch, J. Flood, R. Koha, and D. Ganem.** 1996. The seroepidemiology of human herpesvirus 8 (Kaposi's sarcoma-associated herpesvirus): distribution of infection in KS risk groups and evidence for sexual transmission. Clin. Infect. Dis. **23:**249.
22. **Kudoh, A., M. Fujita, L. Zhang, N. Shirata, T. Daikoku, Y. Sugaya, H. Isomura, Y. Nishiyama, and T. Tsurumi.** 2005. Epstein-Barr virus lytic replication elicits ATM checkpoint signal transduction while providing an S-phase-like cellular environment. J. Biol. Chem. **280:**8156–8163.
23. **Li, M. T., J. MacKey, S. C. Czajak, R. C. Desrosiers, A. A. Lackner, and J. U. Jung.** 1999. Identification and characterization of Kaposi's sarcoma-associated herpesvirus K8.1 virion glycoprotein. J. Virol. **73:**1341–1349.
24. **Liao, W., Y. Tang, S. F. Lin, H. J. Kung, and C. Z. Giam.** 2003. K-bZIP of Kaposi's sarcoma-associated herpesvirus/human herpesvirus 8 (KSHV/HHV-8) binds KSHV/HHV-8 Rta and represses Rta-mediated transactivation. J. Virol. **77:**3809–3815.
25. **Lukac, D. M., J. R. Kirshner, and D. Ganem.** 1999. Transcriptional activation by the product of open reading frame 50 of Kaposi's sarcoma-associated herpesvirus is required for lytic viral reactivation in B cells. J. Virol. **73:**9348–9361.
26. **Lukac, D. M., R. Renne, J. R. Kirshner, and D. Ganem.** 1998. Reactivation of Kaposi's sarcoma-associated herpesvirus infection from latency by expression of the ORF 50 transactivator, a homolog of the EBV R protein. Virology **252:**304–312.
27. **Luna, R. E., F. C. Zhou, A. Baghian, V. Chouljenko, B. Forghani, S. J. Gao, and K. G. Kousoulas.** 2004. Kaposi's sarcoma-associated herpesvirus glycoprotein K8.1 is dispensable for virus entry. J. Virol. **78:**6389–6398.
28. **Matsumura, S., Y. Fujita, E. Gomez, N. Tanese, and A. C. Wilson.** 2005. Activation of the Kaposi's sarcoma-associated herpesvirus major latency locus by the lytic switch protein RTA (ORF50). J. Virol. **79:**8493–8505.
29. **Medveczky, M. M., E. Horvath, T. Lund, and P. G. Medveczky.** 1997. In vitro antiviral drug sensitivity of the Kaposi's sarcoma-associated herpesvirus. AIDS **11:**1327–1332.
30. **Nakamura, H., M. Lu, Y. Gwack, J. Souvlis, S. L. Zeichner, and J. U. Jung.** 2003. Global changes in Kaposi's sarcoma-associated virus gene expression patterns following expression of a tetracycline-inducible Rta transactivator. J. Virol. **77:**4205–4220.
31. **Nealon, K., W. W. Newcomb, T. R. Pray, C. S. Craik, J. C. Brown, and D. H. Kedes.** 2001. Lytic replication of Kaposi's sarcoma-associated herpesvirus results in the formation of multiple capsid species: isolation and molecular characterization of A, B, and C capsids from a gammaherpesvirus. J. Virol. **75:**2866–2878.
32. **Pak, F., P. Pyakural, P. Kokhaei, E. Kaaya, A. A. Pourfathollah, G. Selivanova, and P. Biberfeld.** 2005. HHV-8/KSHV during the development of Kaposi's sarcoma: evaluation by polymerase chain reaction and immunohistochemistry. J. Cutan. Pathol. **32:**21–27.
33. **Parravicini, C., B. Chandran, M. Corbellino, E. Berti, M. Paulli, P. S. Moore, and Y. Chang.** 2000. Differential viral protein expression in Kaposi's sarcoma-associated herpesvirus-infected diseases: Kaposi's sarcoma, primary effusion lymphoma, and multicentric Castleman's disease. Am. J. Pathol. **156:**743–749.
34. **Parsons, C. H., L. A. Adang, J. Overdevest, C. M. O'Connor, J. R. Taylor, D. Camerini, and D. H. Kedes.** 2006. KSHV targets multiple leukocyte lineages during long-term productive infection in NOD/SCID mice. J. Clin. Investig. **116:**1963–1973.
35. **Preston, C. M., and M. J. Nicholl.** 2006. Role of the cellular protein hDaxx in human cytomegalovirus immediate-early gene expression. J. Gen. Virol. **87:**1113–1121.
36. **Raab, M. S., J. C. Albrecht, A. Birkmann, S. Yaguboglu, D. Lang, B. Fleckenstein, and F. Neipel.** 1998. The immunogenic glycoprotein gp35-37 of human herpesvirus 8 is encoded by open reading frame K8.1. J. Virol. **72:**6725–6731.
37. **Rabkin, C. S., R. J. Biggar, M. S. Baptiste, T. Abe, B. A. Kohler, and P. C. Nasca.** 1993. Cancer incidence trends in women at high risk of human immunodeficiency virus (HIV) infection. Int. J. Cancer **55:**208–212.
38. **Rainbow, L., G. M. Platt, G. R. Simpson, R. Sarid, S. J. Gao, H. Stoiber, C. S. Herrington, P. S. Moore, and T. F. Schulz.** 1997. The 222- to 234-kilodalton latent nuclear protein (LNA) of Kaposi's sarcoma-associated herpesvirus (human herpesvirus 8) is encoded by orf73 and is a component of the latency-associated nuclear antigen. J. Virol. **71:**5915–5921.
39. **Renne, R., W. Zhong, B. Herndier, M. McGrath, N. Abbey, D. Kedes, and D. Ganem.** 1996. Lytic growth of Kaposi's sarcoma-associated herpesvirus (human herpesvirus 8) in culture. Nat. Med. **2:**342–346.
40. **Sakakibara, S., K. Ueda, K. Nishimura, E. Do, E. Ohsaki, T. Okuno, and K. Yamanishi.** 2004. Accumulation of heterochromatin components on the terminal repeat sequence of Kaposi's sarcoma-associated herpesvirus mediated by the latency-associated nuclear antigen. J. Virol. **78:**7299–7310.
41. **Sanchez, D. J., L. Coscoy, and D. Ganem.** 2002. Functional organization of MIR2, a novel viral regulator of selective endocytosis. J. Biol. Chem. **277:**6124–6130.
42. **Shaw, R. N., J. L. Arbiser, and M. K. Offermann.** 2000. Valproic acid induces human herpesvirus 8 lytic gene expression in BCBL-1 cells. AIDS **14:**899–902.
43. **Si, M. W., J. Jagirdar, Y. J. Zhang, S. J. Gao, and I. T. Yeh.** 2005. Detection of KSHV in transbronchial biopsies in patients with Kaposi sarcoma. Appl. Immunohistochem. Mol. Morphol. **13:**61–65.
44. **Sun, R., S. F. Lin, L. Gradoville, Y. Yuan, F. X. Zhu, and G. Miller.** 1998. A viral gene that activates lytic cycle expression of Kaposi's sarcoma-associated herpesvirus. Proc. Natl. Acad. Sci. USA **95:**10866–10871.
45. **Sun, R., S. F. Lin, K. Staskus, L. Gradoville, E. Grogan, A. Haase, and G. Miller.** 1999. Kinetics of Kaposi's sarcoma-associated herpesvirus gene expression. J. Virol. **73:**2232–2242.
46. **Suscovich, T. J., M. Paulose-Murphy, J. D. Harlow, Y. D. Chen, S. Y. Thomas, T. J. Mellott, B. D. Walker, D. T. Scadden, S. Zeichner, and C. Brander.** 2004. Defective immune function of primary effusion lymphoma cells is associated with distinct KSHV gene expression profiles. Leuk. Lymphoma **45:**1223–1238.
47. **Taylor, M. M., B. Chohan, L. Lavreys, W. Hassan, M. L. Huang, L. Corey, R. A. Morrow, B. A. Richardson, K. Mandaliya, J. Ndinya-Achola, J. Bwayo, and J. Kreiss.** 2004. Shedding of human herpesvirus 8 in oral and genital secretions from HIV-1-seropositive and -seronegative Kenyan women. J. Infect. Dis. **190:**484–488.
48. **Tomescu, C., W. K. Law, and D. H. Kedes.** 2003. Surface downregulation of major histocompatibility complex class I, PE-CAM, and ICAM-1 following de novo infection of endothelial cells with Kaposi's sarcoma-associated herpesvirus. J. Virol. **77:**9669–9684.
49. **van Engeland, M., L. J. Nieland, F. C. Ramaekers, B. Schutte, and C. P.**

Reutelingsperger. 1998. Annexin V-affinity assay: a review on an apoptosis detection system based on phosphatidylserine exposure. Cytometry **31:**1–9.
50. **Wang, L., N. Wakisaka, C. C. Tomlinson, S. M. DeWire, S. Krall, J. S. Pagano, and B. Damania.** 2004. The Kaposi's sarcoma-associated herpesvirus (KSHV/HHV-8) K1 protein induces expression of angiogenic and invasion factors. Cancer Res. **64:**2774–2781.
51. **White, E. A., C. L. Clark, V. Sanchez, and D. H. Spector.** 2004. Small internal deletions in the human cytomegalovirus IE2 gene result in nonviable recombinant viruses with differential defects in viral gene expression. J. Virol. **78:**1817–1830.
52. **Xu, Y. Y., D. P. AuCoin, A. R. Huete, S. A. Cei, L. J. Hanson, and G. S. Pari.** 2005. A Kaposi's sarcoma-associated herpesvirus/human herpesvirus 8 ORF50 deletion mutant is defective for reactivation of latent virus and DNA replication. J. Virol. **79:**3479–3487.
53. **Yada, K., E. Do, S. Sakakibara, E. Ohsaki, E. Ito, S. Watanabe, and K. Ueda.** 2006. KSHV RTA induces a transcriptional repressor, HEY1 that represses rta promoter. Biochem. Biophys. Res. Commun. **345:**410–418.
54. **Ye, F. C., F. C. Zhou, S. M. Yoo, J. P. Xie, P. J. Browning, and S. J. Gao.** 2004. Disruption of Kaposi's sarcoma-associated herpesvirus latent nuclear antigen leads to abortive episome persistence. J. Virol. **78:**11121–11129.
55. **Yu, Y. M., J. B. Black, C. S. Goldsmith, P. J. Browning, K. Bhalla, and M. K. Offermann.** 1999. Induction of human herpesvirus-8 DNA replication and transcription by butyrate and TPA in BCBL-1 cells. J. Gen. Virol. **80:**83–90.
56. **Zhu, L. J., V. Puri, and B. Chandran.** 1999. Characterization of human herpesvirus-8 K8.1A/B glycoproteins by monoclonal antibodies. Virology **262:**237–249.
57. **Ziegler, J. L., A. C. Templeton, and C. L. Vogel.** 1984. Kaposis sarcoma—a comparison of classical, endemic, and epidemic forms. Semin. Oncol. **11:**47–52.
58. **Zoeteweij, J. P., S. T. Eyes, J. M. Orenstein, T. Kawamura, L. J. Wu, B. Chandran, B. Forghani, and A. Blauvelt.** 1999. Identification and rapid quantification of early- and late-lytic human herpesvirus 8 infection in single cells by flow cytometric analysis: characterization of antiherpesvirus agents. J. Virol. **73:**5894–5902.